Growth Mechanism of Primary and Eutectic TiB_2 Particles in a Hypereutectic Steel Matrix Composite

Z.C. LUO, B.B. HE, Y.Z. LI, and M.X. HUANG

The growth mechanism of primary and eutectic TiB_2 particles in a hypereutectic steel matrix composite (SMC) has been investigated by combining microstructure and crystallographic analysis in the present work. It is found that the TiB_2 particles in the as-cast microstructure have complex morphologies including two kinds of primary particles and several categories of eutectic particles. Twin-induced dendritic growth of primary TiB_2 particles and epitaxial growth of eutectic fibers are found in the present SMC by detailed crystallography analysis. Furthermore, we demonstrate that the crystallographic features strongly affect the solidification process and the final microstructures. Finally, several alloying strategies are proposed to control the solidification microstructure.

DOI: 10.1007/s11661-017-4001-5

I. INTRODUCTION

AN efficient way to reduce automobile emissions is weight reduction which has traditionally been achieved by using advanced high strength steels (AHSS), as higher strength enables the use of thinner components. However, thickness reduction can significantly reduce the stiffness of components.[1–3] For some components such as chassis parts, thickness reduction has now reached its limits due to the demands of high stiffness. Therefore, there is a strong need to develop new AHSS with a higher Young's modulus, which can be achieved by embedding ceramic particles into the steel matrix, forming a steel matrix composite (SMC). It has been demonstrated recently that the SMC reinforced by TiB_2 particles can be produced by eutectic solidification using conventional steel technology, which can ensure low cost and high productivity and therefore enables potential automotive applications.[1,4] Furthermore, the SMC has a lower density compared to conventional AHSS due to the addition of a high volume fraction of low-density TiB_2. Compared with other metal matrix composites (MMC) produced by the powder metallurgy method, the SMC manufactured by eutectic solidification exhibits a much better ductility as the interfaces between the matrix and TiB_2 particles are semi-coherent[5] and can undergo interfacial plasticity prior to interface debonding.[6]

The strength of the SMC depends on the volume fraction and the size of particles.[7,8] However, increasing the volume fraction of TiB_2 will inevitably result in a higher fraction of large primary particles, which leads to significant stress concentration and facilitates nucleation of cracks and hence could be detrimental to the ductility and toughness.[9] Particle refinement, therefore, becomes a promising method to improve the strength of the composite. For such eutectic SMC, the particle size can be refined by controlling the solidification rates.[10] It is noted that an amorphous matrix material with supersaturated solute was obtained from fast solidification (~10^7 K/s). The fine dispersed nano-scaled precipitation of TiB_2 particles was expected to form during the subsequent annealing. However, such fast solidification technique remains a challenge to existing steel industry and is not suitable for mass production at present.

Another way to control the particle size is using alloying elements. Some elements, such as Mo, Mn, Al, and Ta, have demonstrated their capability to refine eutectic particles.[11] However, the mechanism for such refinement is still not clear. Normally, the anisotropic growth nature of ceramic phase in metal/ceramic eutectic solidification systems will make the phase diagram diverge greatly from equilibrium state.[12–15] In other words, the crystallographic factors could affect the solidification process and determine the final microstructure.[12,16–20] Inspired by these studies,[12–20] here we propose that the growth of primary and eutectic TiB_2 particles in the current SMC may depend on their crystallographic features. But the crystallographic-related growth mechanism of TiB_2 particles is still unclear in the field. In this paper, the three-dimensional morphology of these particles in an as-cast composite has been revealed by electron microscopy after a deep etching treatment. Furthermore, the crystallographic features and microstructure of TiB_2 particles are revealed by electron backscattered diffraction (EBSD) and transmission electron microscopy (TEM). Then the growth mechanisms of the TiB_2 particles and the possible alloying strategies are discussed.

Z.C. LUOIS, B.B. HE, Y.Z. LI, and M.X. HUANG are with the Shenzhen Institute of Research and Innovation, the University of Hong Kong, Shenzhen, 518000, China, and also with the Department of Mechanical Engineering, The University of Hong Kong, Hong Kong. Contact e-mail: mxhuang@hku.hk
Manuscript submitted September 15, 2016.
Article published online February 7, 2017

II. MATERIALS AND EXPERIMENTS

The SMC sample with chemical composition of Fe-6Ti-2.2B-0.2Nb (in wt pct) is investigated in the present work. The material was prepared using FeTi, FeB, and pure iron powders melted at 1923 K (1650 °C) and then solidified at a constant slow cooling rate of 1 K/s in a vacuum environment. A small amount of Nb was added into the powder mixture to minimize the formation of TiC. The SMCs can be produced by eutectic solidification as experimentally proved by a previous study.[6]

The EBSD measurement was performed in Leo 1530 at 20 kV with a step size varied between 0.1 and 0.5 μm and the corresponding data were processed by HKL Channel 5. The sample for EBSD observation was prepared by vibration polishing using SiO_2 suspensions for 2 hours. To reveal the 3-D microstructure of TiB_2 particles, the well-polished sample was immersed in the hydrochloric acid solution (~30 pct in concentration) for about 3 hours. Then the sample was washed by pure water and ethanol several times to remove the residual hydrochloric acid. Finally, the sample was dried out by warm blow carefully. The scanning electron microscopy (SEM) observation was carried out on the deeply etched sample in the Leo 1530 FEG-SEM at 5 kV. The TEM observation was performed in FEI Tecnai G20 at 200 kV. The TEM sample was prepared by FEI Quanta 200 focus ion beam (FIB) milling.

III. RESULTS

Figure 1 shows the microstructure of as-cast SMC. The TiB_2 particles are confirmed by EBSD phase mapping (Figures 1(b1) and (b2)) and element mapping (Figure 1(c2) and (c3)). The larger particles are the primary TiB_2 particles. Accompanied these primary particles, large ferrite grains (some of them like halos around the primary TiB_2 particles) have been observed as marked by arrows in Figure 1(a). According to the orientation of ferrite phase, the eutectic colonies can be identified as shown in Figure 1(b1). Within one colony, the eutectic TiB_2 particles have an indistinguishable orientation as highlighted in Figure 1(b2). It suggests that the eutectic TiB_2 particles may maintain a given crystallographic orientation during solidification.

Figure 2 reveals the 3-D morphology of TiB_2 particles. The primary hexagonal prisms of TiB_2 particles (Figure 2(b)) are embedded in the eutectic colonies. The eutectic TiB_2 particles, however, are either plate-like or fiber-like as shown in Figure 2(c). Furthermore, pieces of comb-like eutectic TiB_2 particles are also observed (Figure 2(d)). The size and interval spacing of latter eutectic phase are much smaller than that of the former ones. Figures 2(b) through (d) shows the morphology of primary particles, 1st eutectic particles, and 2nd eutectic particles, respectively. Interestingly, some of the eutectic TiB_2 particles nucleate and stretch out from the primary particles as shown in Figures 2(e) and (f).

Figure 3 displays the morphology of primary TiB_2 particles. During solidification, the primary TiB_2 particles will float up to the surface of the ingot due to their lower density (about 4.50 g/cm^3[21]) compared to iron liquid (about 7.80 g/cm^3). Most of these particles are hexagonal prisms (Figure 3(a)). One particle was selected for the EBSD mapping. The inverse pole figure (IPF) shows that the top surface of this particle is (0001) crystal plane. Furthermore, the top view of this particle is coincident well with the shape of crystal unit cell (Figure 3(b)). Thus, this primary TiB_2 particle is confirmed as a single crystal, whose top surface is (0001), and the six side surfaces belong to {10-10} type.

However, some primary TiB_2 particles are not single crystals. Figure 4 shows the microstructure of one primary TiB_2 particle with a dendrite. Pole figures extracted from the EBSD data are used instead as shown in Figure 4. This dendrite TiB_2 particle contains two wedge grains (marked B and C in Figure 4(a)). The misorientation angles between grains A/B and grains A/C are both around 70 deg (Figure 4(b)). As proved by the pole figures, grain A and B have two paralleled {10-11} planes and one {11-20} plane. This relationship is also valid between A and C. The orientations of these three grains are shown in Figure 4(c). The possible spatial configurations of these three crystals are schematically reconstructed as revealed on the top left of Figure 4(c). In this case, grain B and C grow from the next two nearest prismatic planes of grain A.

Figure 5(b) shows the {10-10} and (0001) pole figures of TiB_2 particles within two selected regions as marked in Figure 5(a). In these areas, the eutectic TiB_2 particles nucleate from the basal plane of the primary particle. Then the branches grow during solidification. The {10-10} and (0001) pole figure of the TiB_2 particles shows that these TiB_2 particles in the two selected areas have identical orientations (the difference of Euler angle is within 2 deg). The result suggests that no fault forms during the nucleation and growth of TiB_2 eutectic fibers. Figure 6 reveals the microstructure of one eutectic TiB_2 fiber. The presence of axial line defects in the middle of eutectic fiber indicates that the fibers are formed by a spiral growth mechanism, *i.e.*, Frank's spiral growth mechanism.[22] Such line defects should contain a screw dislocation component. The atom stairs caused by the screw dislocation in (0001) plane makes the deposition of material from the melt to this plane much faster than other planes, resulting in the directional growth of TiB_2 eutectic fiber along [0001] direction.

Figure 7 presents the crystallography relationships between eutectic TiB_2 phase and ferrite phase. Within this area, there are four eutectic colonies as marked by Greek letters. The crystallography relationships between TiB_2 and ferrite are revealed by pole figures of each phase as shown in Figure 7. We present the pole figures of two orthogonal planes of each phase. The indices of directions in TiB_2 phase are directly deduced from the planes because they are parallel to the basal plane in the present study. Some relationships are confirmed, such as Potter orientation relationship:[23] $(01\text{-}11)_{hcp}//(110)_{bcc}$ and $[2\text{-}1\text{-}10]_{hcp}//[1\text{-}11]_{bcc}$, or $(0001)_{hcp}//(011)_{bcc}$ and $[10\text{-}10]_{hcp}//[1\text{-}11]_{bcc}$. However, no global representative crystallography relation between the two eutectic phases can be identified.

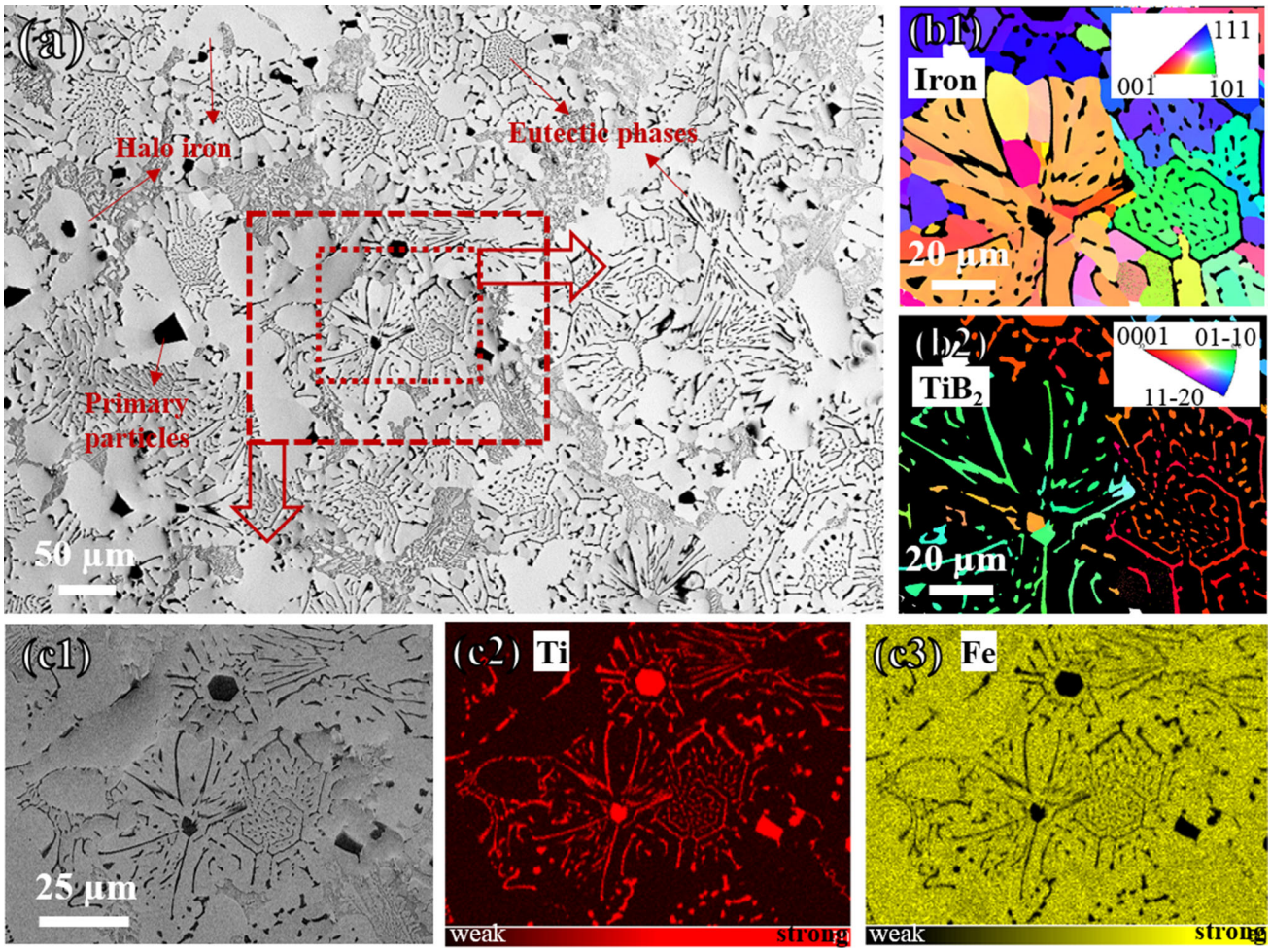

Fig. 1—(*a*) SEM image of the as-cast *in situ* TiB_2/iron composite; (*b1*) and (*b2*) EBSD inverse pole figure map of iron phase and TiB_2 phase, respectively; (*c2*) and (*c3*) EDX map of Ti and Fe elements of areas (*c1*). For the color images, please refer to the online version of this article.

IV. DISCUSSION

The above results indicate that the microstructures of the present SMC are complex and can be separated into three parts: primary TiB_2 particles (accompanied by halo iron phase), 1st eutectic particles, and 2nd eutectic particles as shown in Figures 1 and 2. It suggests a stepwise solidification behavior as revealed schematically in Figure 8. At the beginning of solidification, the primary TiB_2 particles are formed firstly due to the normal solidification nature of hyper-eutectic melt. As the primary TiB_2 particles grow, the solute concentration around such particles will decrease, leading to the nucleation of iron phase before the cooperative growth of eutectic phases (Figure 8(b)). The eutectic TiB_2 particles can either nucleate at the basal plane of the primary TiB_2 particles or on the halo iron phase as shown in Figures 1, 2 and 4. At last, liquid phase islands which are surrounded by solidified phase (Figure 8(c)) are left. Interestingly, TiB_2 phase then nucleates in the center of these liquid islands and grows like a feather (Figure 8(d)). The size and internal spacing of TiB_2 in these zones are much smaller than that in the 1st eutectic microstructure, as shown in Figures 2(c) and (d).

Whether this feathery lamellar structure is eutectic non-facet phase is still controversial. Weiss and Loper[24,25] suggested that the similar lamellar morphology in hyper-eutectic Al-Si system was a structure between primary and eutectic structure. Because the spines of such structure can grow from the branch of star-shaped Si crystal (primary phase). However, the lamellar structure in the present study is independent of the primary phase as shown in Figure 2. We suggest that this lamellar structure belongs to eutectic phase for the following reasons. First, based on Croker's work,[26] the eutectic morphology may become complex regular (*e.g.*, lamellar structure surrounded by irregular structure) with increasing volume fraction of the facet phase at a given growth rate. Second, the 2nd eutectic reaction occurs at lower temperature and thus larger undercooling condition. Therefore, the growth velocity becomes higher and yields a finer inter-lamellar spacing eutectic microstructure.[27]

This stepwise solidification behavior can be interpreted by the coupled growth zone mechanism on the basis of Fe-TiB_2 pseudo phase diagram.[4,10] The coupled growth zone defines the alloy compositions and interface undercooling conditions at which the growth

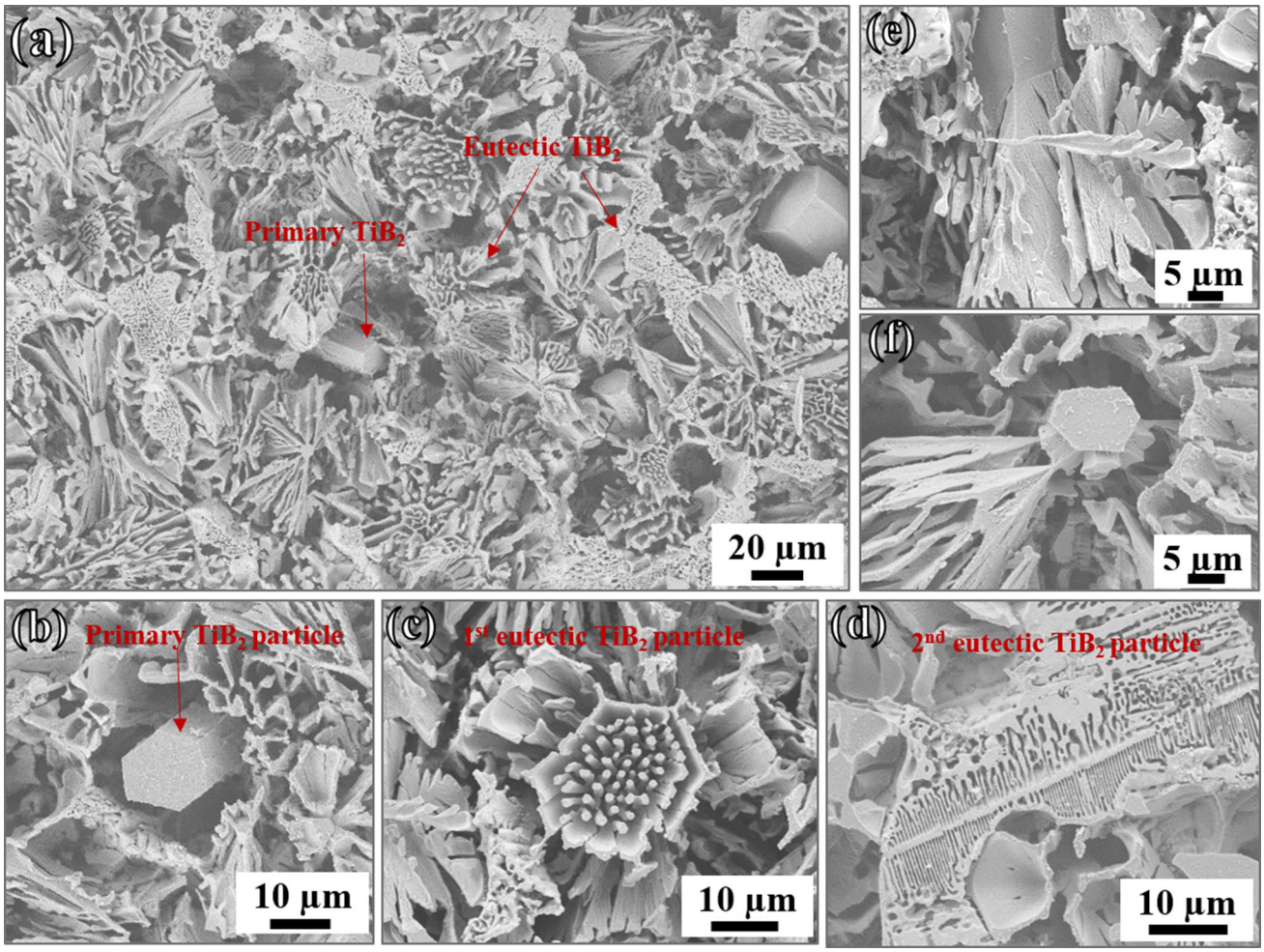

Fig. 2—3-D morphology of TiB_2 particles: (*a*) full view of the TiB_2 phase skeleton; (*b*) hexagonal prisms of primary TiB_2; (*c*) fiber or plate-like eutectic TiB_2; (*d*) lamellar eutectic TiB_2; (*e*) and (*f*) eutectic TiB_2 grown from basal plane and prismatic plane of primary TiB_2 particles, respectively.

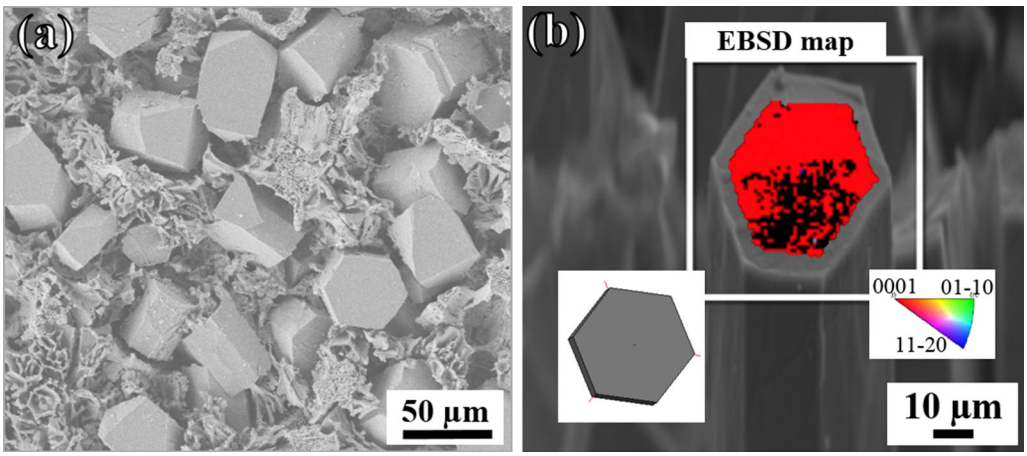

Fig. 3—(*a*) TiB_2 primary near the ingot surface; (*b*) EBSD inverse pole figure of one upright primary particle. For the color images, please refer to the online version of this article.

rate of eutectic phases exceeds that of either single phase.[13,28,29] In the present system, TiB_2 has much higher fusion temperature and tends to grow anisotropically into faceted crystals. Hence, it requires more undercooling for its growth than that of the iron phase. Consequently, the coupled growth region of

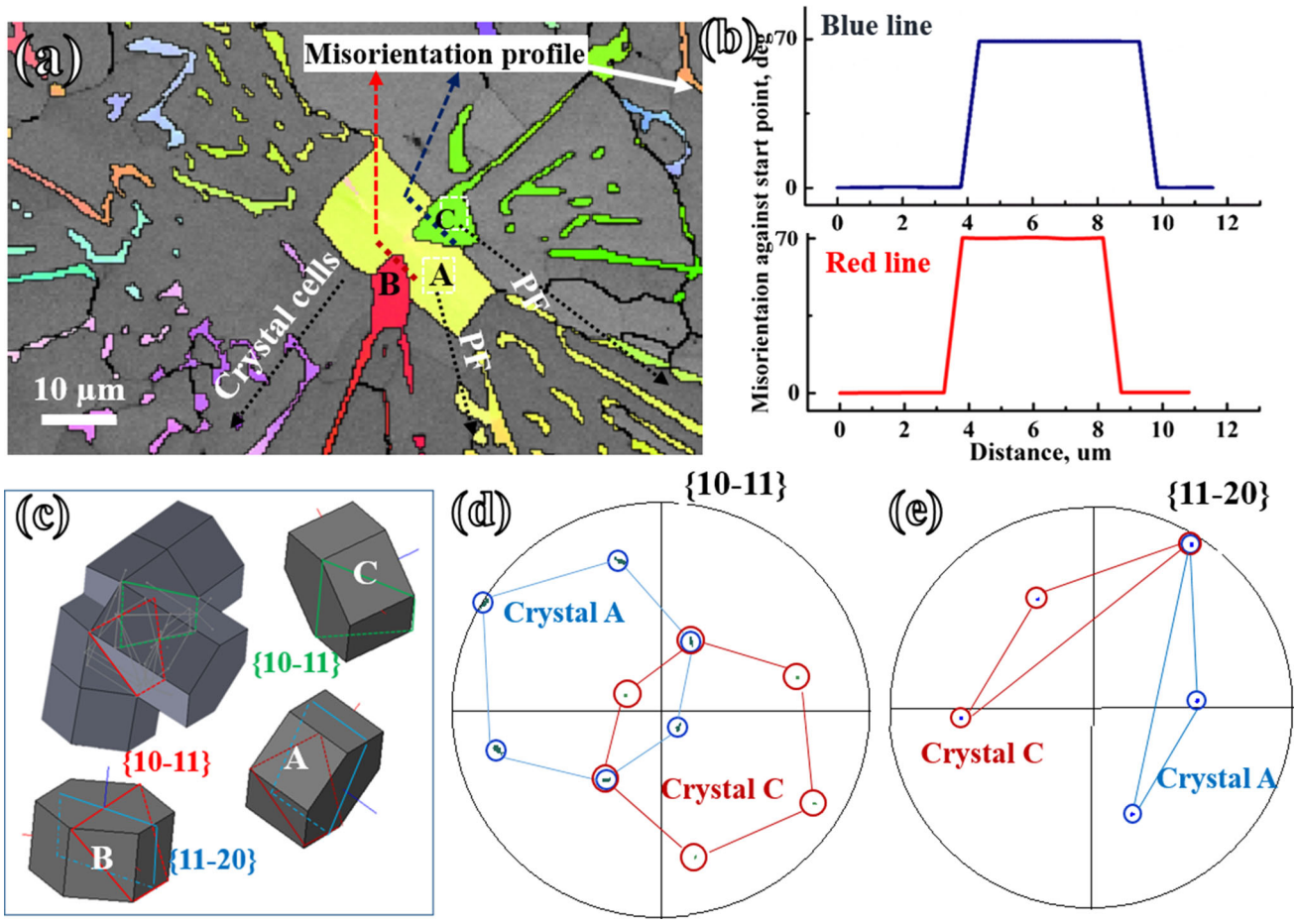

Fig. 4—(*a*) IPF color map of TiB_2 particles; (*b*) misorientation profiles against the start point of the two lines crossing grain B and grain C; (*c*) crystal cells of grain A, B, and C, and the possible spatial configuration; (*d*) and (*e*) {10-11} and {11-20} pole figures of grain A and grain C. For the color images, please refer to the online version of this article.

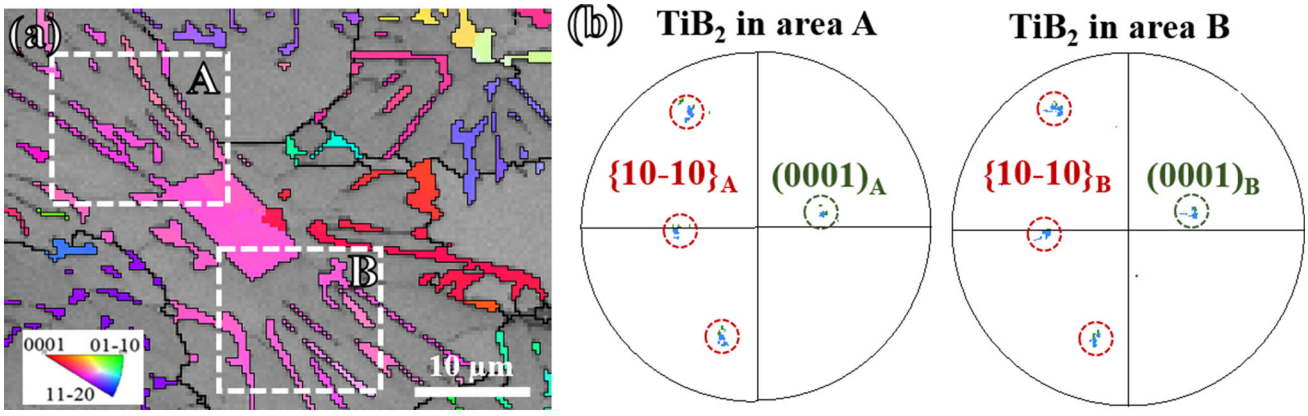

Fig. 5—(*a*) IPF color mapping of TiB_2 phase; (*b*) the {10-10} and (0001) pole figures of the TiB_2 phase within the selected area as marked out in (a). For the color images, please refer to the online version of this article.

Fe-TiB_2 system diverges to the side of TiB_2 as shown in Figure 9. During solidification, the primary TiB_2 particles form firstly; the solute concentration of the liquid around primary particles will decrease by following the liquidus line until the formation of halo iron (at point C).

The formation of halo iron is a result of no-reciprocal nucleation characteristics, which indicates that one eutectic phase will act as an effective heterogeneous nucleation site for the other phase, but not *vice versa*.[28] In the present Fe-TiB_2 system, the primary TiB_2 particles may be poor nucleus for iron, so that the

eutectic growth will be delayed and the liquid phase around the primary particles becomes severely undercooled and iron enriched. This leads to the growth of large iron grain. Similar halo phase has also been observed in off-eutectic iron-aluminide/TiC composites.[13,14]

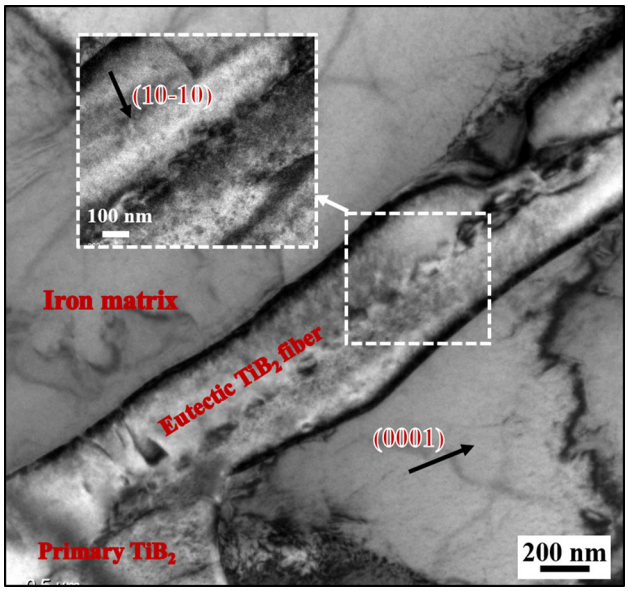

Fig. 6—TEM bright field image of the eutectic fiber at two different *g* vector operating conditions, showing spiral line defects in the center of the fiber.

As mentioned before, the growth of ceramic crystal in the liquid is directional.[12,20] The close-packed plane grows with the lower velocity because this plane has fewer holes or pockets available for the accommodation of a liquid atom as it joints to crystal.[30] For TiB_2 crystal, the close-packed plane and next close-packed plane are (0001) (d = 0.323 nm) and {10-10} (d = 0. 263 nm), respectively.[21] Thus, these two planes should grow slowest. Figure 10(a) shows the possible growth mechanism of hexagonal primary TiB_2 particles. The inclined plane (less close-packed plane) grows faster than the basal and prismatic planes. However, this fast-grow plane will gradually grow itself out of existence, leaving behind the close-packed planes as the particle surfaces.[31]

For dendritic primary TiB_2 particles, the trunk grains and dendrite grains are symmetrical with {10-11} twin boundaries as revealed in Figure 4(c). Indeed, the formation of growth twins in the crystal during solidification could be achieved by two mechanisms, namely layered growth[32] and twin plane re-entrant (TPRE) edge growth.[16,20,33,34] The layered growth mechanism is adopted to explain the experimental findings in this paper. As mentioned before, the {10-11} planes in TiB_2 phase grow faster than the basal and prismatic planes. It is considered that a twin nucleus occurs due to the

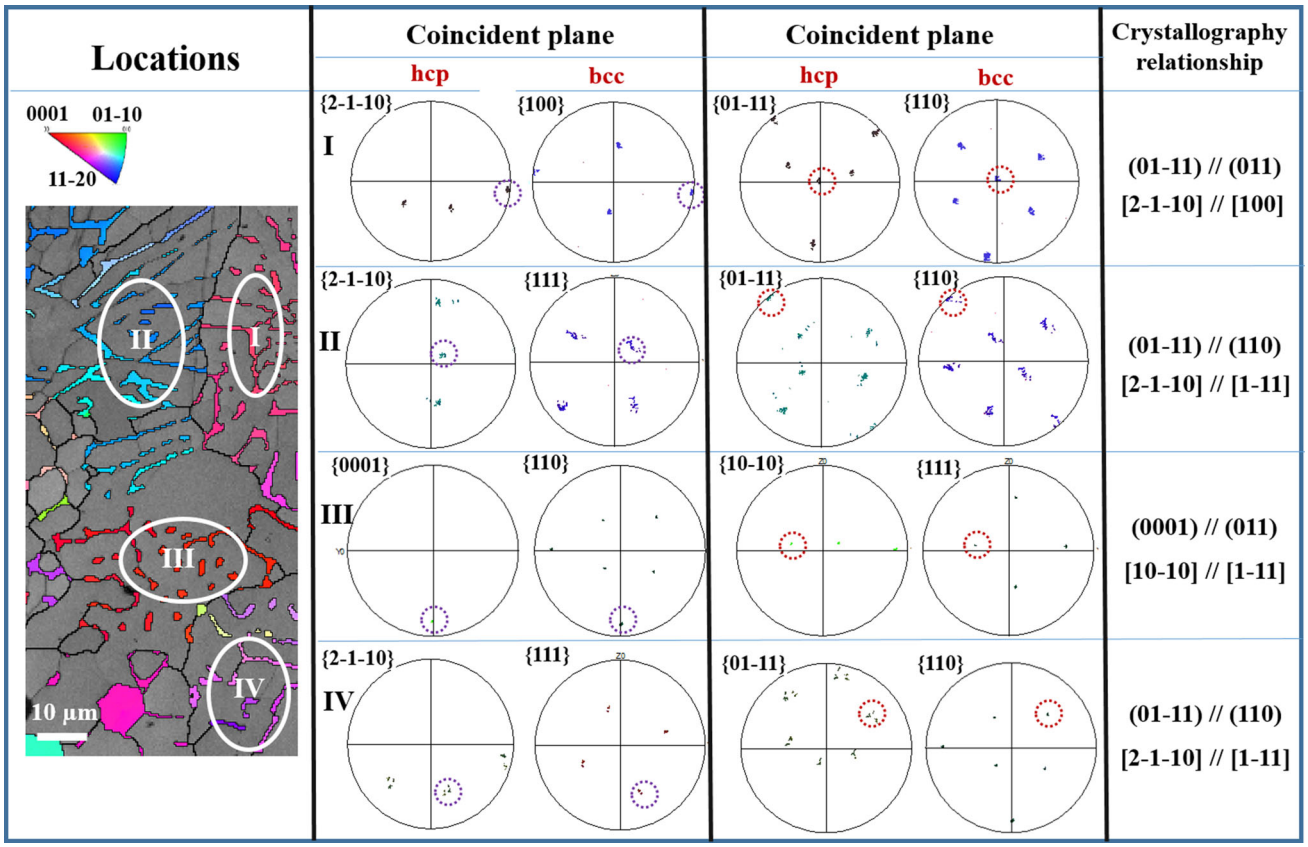

Fig. 7—Crystallography relationship between eutectic TiB_2 and ferrite phase represented by pole figures of each phase in four eutectic colonies. For the color images, please refer to the online version of this article.

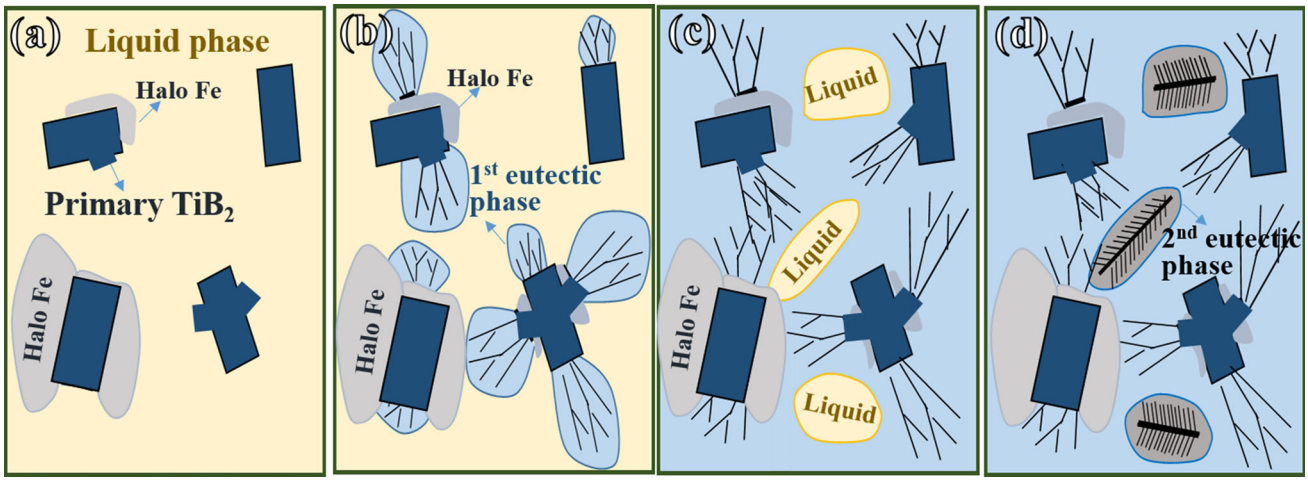

Fig. 8—Schematic diagram showing the solidification processes of the present SMC: (*a*) the growth of primary TiB_2 particles and halo rion phase; (*b*) nucleation and growth of the eutectic phase; (*c*) the liquid phase islands surrounded by eutectic colonies; (*d*) the comb-like eutectic phases in the liquid phase islands. For the color images, please refer to the online version of this article.

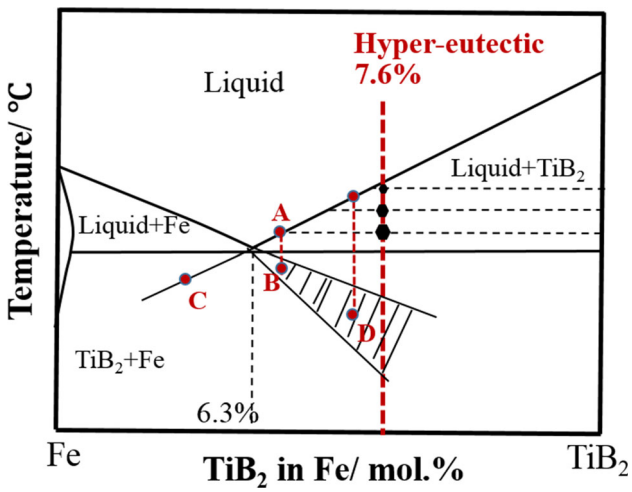

Fig. 9—Schematic of asymmetrical cooperative precipitation zone.

faulted deposition of atomic layers on the front. Then the continuous deposition of atoms from the melt on this faulted layer forms one dendrite grain. This mechanism is illustrated schematically in Figure 10(b). The (10-11) plane grows initially along [10-10] direction of the trunk grain, but this growth is thermodynamically unfavorable due to the resultant high concentration gradient of solute in front of the solid-liquid interface. Then a fault gradually forms and the growth direction changes to the [10-10] of the dendrite grain.

The formation of dendrite particles can decrease the size of primary TiB_2 particles as well as restrict the formation of halo iron phase. Figure 10(c) shows size distribution of the primary TiB_2 particles with and without dendrite grains. SEM images of two typical particles are provided at the inset of Figure 10(b). Considering the high aspect ratio of some particles, we measure the largest and smallest lengths at two orthogonal directions for each particle. The results show that the size distribution of dendritic primary particles is single peak within the range of 0–20 μm. But for the dendrite-free particles, two separated distribution peaks are observed and more than 40 pct are larger than 20 μm. It suggests that the aspect ratio of dendrite free primary particles is much higher than that of dendritic particles. Furthermore, the mean size of the primary particles with dendrite grains is about 11 μm while the ones without dendrite grains is about 18 μm. This can be interpreted *via* the coupled growth zone theory. With the help of more basal planes serve as possibilities for the eutectic TiB_2 to nucleate, the constitution-temperature path along the liquidus line can be interrupted at point A (Figure 9), steps into the zone of asymmetrical cooperative precipitation, reaches point B, where the eutectic structure is kinetically favored. Otherwise, the given undercooling condition cannot satisfy the nucleation requirement for the eutectic phase. Then the liquid will undercool following the liquidus line until reaching point C, resulting in the appearance of halo iron phase and further directional growth of primary TiB_2 crystals.

The eutectic TiB_2 particles can nucleate on the (0001) plane of either single-crystal or dendrite primary particles. Once they nucleate, the eutectic TiB_2 particles grow in an anomalous way. As shown in Figure 2, the eutectic particles present complex features (fibers, plates, and feathers), and have a wide range of inter-rod/-lamellar spacing. To gain a better understanding of the various interlamellar spacing between TiB_2 eutectic particles, we can apply the scaling laws developed by Jackson and Hunt[27] to describe the eutectic growth behavior qualitatively. This law relates the lamellar/rod spacing to the growth rate V and the local undercooling at the growth front ΔT_f *via*,

$$\Delta T_f = K_1 V\lambda + \frac{K_2}{\lambda}, \qquad [1]$$

where K_1 and K_2 are material-dependent parameters. Under certain growth rate, we have the spacing-undercooling relationship as schematically shown in Figure 11(a). The optimum interlamellar spacing λ_a, corresponding to the minimum undercooling value (ΔT_f) for a given growth rate in metal–metal eutectic.[28]

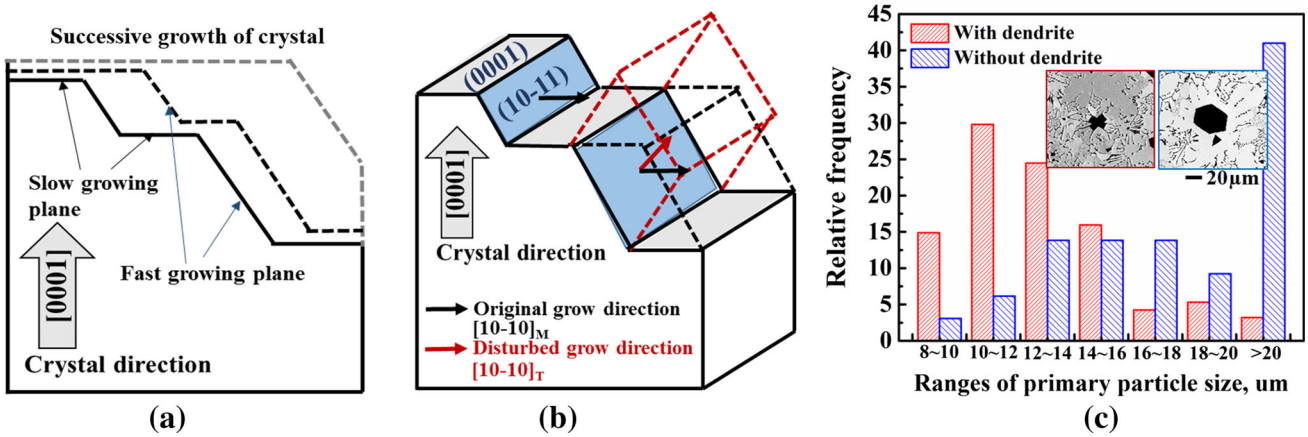

Fig. 10—(*a*) Growth mechanism of single crystal primary TiB_2 particles; (*b*) growth mechanism of dendrite primary TiB_2 particles; (*c*) size distribution of the primary TiB_2 particles with and without dendrite grains.

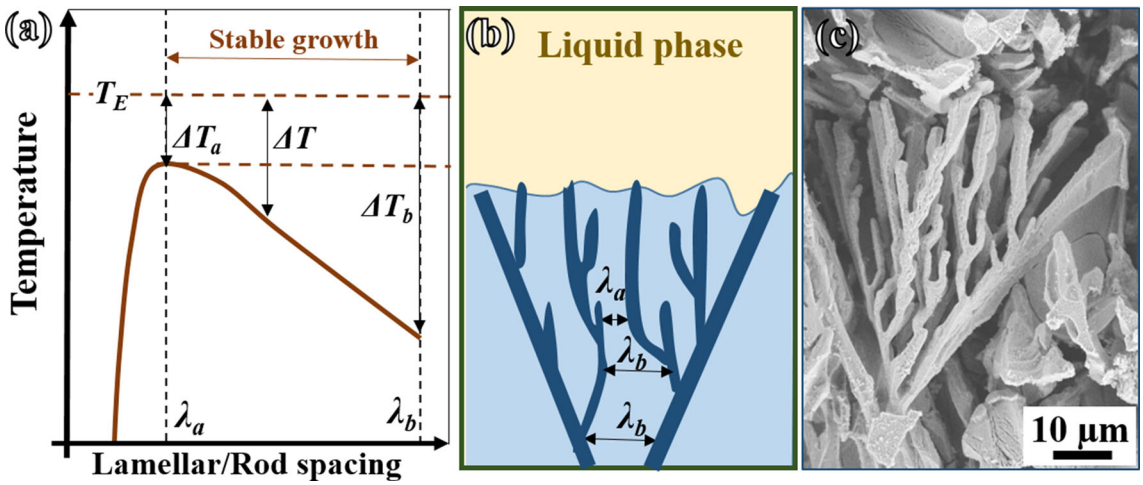

Fig. 11—(*a*) The spacing-undercooling relationship under certain growth rate according to Eq. [1]; (*b*) schematic diagram showing growth mechanism of the coral-like TiB_2 eutectic; (*c*) typical morphology of fiber eutectic TiB_2.

In metal–ceramic eutectic system, this optimum value represents a minimum possible value of local spacing.[35] Figure 11(b) is the schematic diagram revealing the growth process of coral-like eutectic TiB_2 phase as shown in Figure 11(c). With the growth of eutectic fiber, the diffusion path of solute increases, resulting in a higher concentration at the solid-liquid front between two rods. Upon a certain value (λ_b), the increased constitutional undercooling contributes to the branching growth of eutectic TiB_2. The crystal orientations of the eutectic TiB_2 fibers are identical because they are formed by a spiral growth mechanism along [0001] direction. Within one eutectic grain, the free energy of the interphase boundary between the two solids keeps constant because each phase has a fixed lattice orientation. There exist one or several families of coincident planes for each eutectic phase which corresponds to the minimal values of interphase boundary energy.[15] Therefore, certain crystallography relationships are observed within the eutectic colonies as shown in Figure 7.

Generally, the morphologies of crystals in the melt are determined by the crystal structure (the internal factors) and the crystal growth conditions (the external factors). Without disturbance, the internal factors will lead to an equilibrium crystal shape with minimum total surface free energy.[36] Therefore, most of the primary TiB_2 particles are perfect hexagonal prisms (Figures 2 and 3), with their lowest surface energy planes: (0001) and {10-10} planes exposing as surfaces. However, this growth process can be influenced by additives (external factors) intentionally added into the melt. It is suggested that some impurities can poison the active sites in the fast growth crystal planes. This effect will retard the growth rate of these planes and therefore result in the modification of morphologies.[37,38]

The high aspect ratio of dendrite-free primary particles and eutectic fibers will be crushed and squeezed during the rolling process leading to the formation of [0001]//RD texture and the introduction of clean surfaces with sharp corners to the particles. The sharp corners could generate significant stress concentration

which favors crack nucleation and thus are detrimental to the ductility. Eliminating these particles should be a key issue for the alloying design. In the present SMC, the disturbed layered-growth of {10-11} planes leads to the formation of twin dendrite primary particles as shown in Figures 2(f) and 5, which can reduce the size and aspect ratio of the primary particles. Such dendritic growth may be due to the addition of Nb. Other elements, such as Si, are supposed to increase the dendritic growth tendency as they can be preferentially adsorbed on the {10-11} planes of TiB_2 crystal.[31] The eutectic TiB_2 fibers grow along [0001] direction by a spiral growth mechanism as proved. The effect of strontium on the eutectic silicon fibers in Al-Si alloy is significant as reported in the literature.[12,20,27] Similar effective modifiers could be found for the Fe-Ti-B system. According to the present study, such modifier should be preferentially adsorbed on the (0001) plane so that the continuous spiral growth of eutectic fiber can be inhibited.

V. CONCLUSIONS

The present work investigates the microstructure and anisotropic solidification behavior of TiB_2 particles in an SMC. The results show that the as-cast SMC contains complex microstructures due to the stepwise solidification processes. The processes contain the formation of primary TiB_2 particles and halo iron phase, followed by the nucleation and growth of fiber or plate eutectic particles, and the formation of laminate eutectic phases. These stepwise processes can be interpreted by the coupled growth zone mechanism and the effect of crystallographic features. Specifically, the primary TiB_2 particles contain two kinds of morphologies: perfect and dendritic hexagonal prisms. The dendritic grains, which are formed by a faulted layered growth mechanism, hold a twin relationship with the trunk grains. Furthermore, the eutectic TiB_2 fibers can nucleate on the (0001) planes of the primary TiB_2 particles. These fibers grow along [0001] direction by a spiral growth mechanism. Therefore, within one eutectic colony, the eutectic TiB_2 particles have identical orientation and may possess certain crystallography relationships with the ferrite phase.

ACKNOWLEDGMENTS

M.X. Huang acknowledges the support from the Steel Joint Funds of the National Natural Science Foundation of China (Grant No. U1560204) and the support from Research Grants Council of Hong Kong (Grants Nos. HKU719712E, HKU712713E).

REFERENCES

1. R. Rana: *Can. Metall. Q.*, 2014, vol. 53, pp. 241–42.
2. S. Pramanik, S. Suwas, and R.K. Ray: *Can. Metall. Q.*, 2014, vol. 53, pp. 274–81.
3. S. Münstermann, Y. Feng, and W. Bleck: *Can. Metall. Q.*, 2014, vol. 53, pp. 264–73.
4. F. Bonnet, V. Daeschler, and G. Petitgand: *Can. Metall. Q.*, 2014, vol. 53, pp. 243–52.
5. S. Lartigue-Korinek, M. Walls, N. Haneche, L. Cha, L. Mazerolles, and F. Bonnet: *Acta Mater.*, 2015, vol. 98, pp. 297–305.
6. M.X. Huang, B.B. He, X. Wang, and H.L. Yi: *Scripta Mater.*, 2015, vol. 99, pp. 13–16.
7. R. Arsenault, L. Wang, and C. Feng: *Acta Metall. Mater.*, 1991, vol. 39, pp. 47–57.
8. N. Ramakrishnan: *Acta Mater.*, 1996, vol. 44, pp. 69–77.
9. Y.Z. Li, Z.C. Luo, H.L. Yi, M.X. Huang, *Metall. Mater. Trans. E* 2016, pp. 1–6.
10. H. Springer, R. Aparicio Fernandez, M.J. Duarte, A. Kostka, and D. Raabe: *Acta Mater.*, 2015, vol. 96, pp. 47–56.
11. R. Aparicio-Fernández, H. Springer, A. Szczepaniak, H. Zhang, and D. Raabe: *Acta Mater.*, 2016, vol. 107, pp. 38–48.
12. A.H.M.G. Day: *Proc. R. Soc. Lond. Ser. A, Math. Phys. Sci.*, 1968, vol. 305, pp. 473–91.
13. S.H. Ko and S. Hanada: *Intermetallics*, 1999, vol. 7, pp. 947–55.
14. S. Kobayashi, A. Schneider, S. Zaefferer, G. Frommeyer, and D. Raabe: *Acta Mater.*, 2005, vol. 53, pp. 3961–70.
15. S. Akamatsu, M. Plapp, *Curr. Opin. Solid State Mater. Sci.* 2015, pp. 1–26.
16. S.-Z. Lu and A. Hellawell: *MTA*, 1987, vol. 18, pp. 1721–33.
17. Y.T. Pei and J.T.M. De Hosson: *Acta Mater.*, 2001, vol. 49, pp. 561–71.
18. S. Shankar, Y.W. Riddle, and M.M. Makhlouf: *Acta Mater.*, 2004, vol. 52, pp. 4447–60.
19. Y. Zhang, H. Zheng, Y. Liu, L. Shi, R. Xu, and X. Tian: *Acta Mater.*, 2014, vol. 70, pp. 162–73.
20. X. Liu, Y. Zhang, B. Beausir, F. Liu, C. Esling, F. Yu, X. Zhao, and L. Zuo: *Acta Mater.*, 2015, vol. 97, pp. 338–47.
21. R.G. Munro: *J. Res. Nat. Inst. Stand. Technol.*, 2000, vol. 105, pp. 709–20.
22. D.R. Veblen and J.E. Post: *Am. Miner.*, 1983, vol. 68, pp. 790–803.
23. M.X. Zhang and P.M. Kelly: *Acta Mater.*, 2005, vol. 53, pp. 1073–84.
24. H. Yi and D. Zhang: *Mater. Lett.*, 2003, vol. 57, pp. 2523–29.
25. J. Weiss and C. Loper: *AFS Trans.*, 1987, vol. 32, pp. 51–62.
26. M. Croker, R. Fidler, and R. Smith: *Proc. R. Soc. Lond. A: Math. Phys. Eng. Sci.*, 1973, vol. 335, pp. 15–37.
27. K. Jackson and J. Hunt: *AIME Met. Soc. Trans.*, 1966, vol. 236, pp. 1129–42.
28. S.T. Bluni, M.R. Notis, and A.R. Marder: *Acta Metall. Mater.*, 1995, vol. 43, pp. 1775–82.
29. H.V.G.M.M. Makhlouf: *J. Light Met.*, 2001, vol. 1, pp. 199–218.
30. R.E. Reed-Hil: *Physical Metallurgy Principles*, 1st ed., Van Nostrand Reinhold Company Co., New York, NY, 1973, pp. 375–76.
31. J. Sun, X. Zhang, Y. Zhang, N. Ma, and H. Wang: *Micron*, 2015, vol. 70, pp. 21–25.
32. S.H. Davis: *Theory of Solidification*, Cambridge University Press, Cambridge, 2001.
33. L. Yang, S. Li, X. Chang, H. Zhong, and H. Fu: *Acta Mater.*, 2015, vol. 97, pp. 269–81.
34. M.A. Salgado-Ordorica and M. Rappaz: *Acta Mater.*, 2008, vol. 56, pp. 5708–18.
35. D.J. Fisher and W. Kurz: *Acta Metall.*, 1980, vol. 28, pp. 777–94.
36. C. Li, Y.Y. Wu, H. Li, and X.F. Liu: *Acta Mater.*, 2011, vol. 59, pp. 1058–67.
37. L. Chen, H.-Y. Wang, Y.-J. Li, M. Zha, and Q.-C. Jiang: *CrystEngComm*, 2014, vol. 16, pp. 448–54.
38. N. Kubota and J.W. Mullin: *J. Cryst. Growth*, 1995, vol. 152, pp. 203–08.